Chin. Phys. Lett. **39**, 057801 (2022) **Express Letter**

Phase-Locking Diffusive Skin Effect

Pei-Chao Cao(曹培超)[1], Yu-Gui Peng(彭玉桂)[1], Ying Li(李鹰)[2,3,4*], and Xue-Feng Zhu(祝雪丰)[1*]

[1]*School of Physics and Innovation Institute, Huazhong University of Science and Technology, Wuhan 430074, China*
[2]*Interdisciplinary Center for Quantum Information, State Key Laboratory of Modern Optical Instrumentation, ZJU-Hangzhou Global Scientific and Technological Innovation Center, Zhejiang University, Hangzhou 310027, China*
[3]*International Joint Innovation Center, Key Laboratory of Advanced Micro/Nano Electronic Devices & Smart Systems of Zhejiang, The Electromagnetics Academy at Zhejiang University, Zhejiang University, Haining 314400, China*
[4]*Jinhua Institute of Zhejiang University, Zhejiang University, Jinhua 321099, China*

(Received 4 March 2022; accepted 2 April 2022; published online 12 April 2022)

We explore the exceptional point (EP) induced phase transition and amplitude/phase modulation in thermal diffusion systems. We start from the asymmetric coupling double-channel model, where the temperature field is unbalanced in the amplitude and locked in the symmetric phase. By extending into the one-dimensional tight-binding non-Hermitian lattice, we study the convection-driven phase locking and the asymmetric-coupling-induced diffusive skin effect with the high-order EPs in static systems. Combining convection and asymmetric couplings, we further show the phase-locking diffusive skin effect. Our work reveals the mechanism of controlling both the amplitude and phase of temperature fields in thermal coupling systems and has potential applications in non-Hermitian topology in thermal diffusion.

DOI: 10.1088/0256-307X/39/5/057801

In the past decade, thermal metamaterials have gained a great deal of attention in meta-device designs for their capacity of regulating the heat flow at will, ranging from microscopic phonon systems to macroscopic diffusive systems.[1−4] Some successful examples include reversibly folding graphene-sheet-adjusted thermal resistor,[5] hydrogel-based thermal switch,[6] coordinate-transformation-based thermal cloak,[7,8] radiative thermal camouflager,[9] and memory-alloy-based thermal diode.[10] Despite the versatile devices with very powerful functionalities, the thermal conductivity modulation is however restricted by the tight choices of natural materials. On the other hand, the thermal convection, which can be flexibly controlled by the mechanical movement, was introduced by researchers to regulate heat flow without this limitation, for example, the convection-based zero-index thermal metamaterial cloaking[11] and the flow-based thermal nonreciprocity.[12−15] Moreover, we can achieve nonreciprocal asymmetric thermal couplings by introducing a convection flow as the bias field in a three-port scattering system. In recent years, the non-Hermitian physics and some related applications have been fully explored in thermal systems, as inspired from non-Hermitian wave systems. Basically, there are two approaches to realize non-Hermitian wave systems. One is by introducing a gain and/or loss material, the other is by using the asymmetric coupling.[16−22]

In a thermal system that is inherently dissipative or non-Hermitian, the wave oscillation can be equivalently mimicked with utilization of opposite thermal convections.[23−30] For example, the anti-parity-time (APT) symmetry with the phase transition at the exceptional point (EP) can be constructed by using two contacted and oppositely moving coupled-ring channels.[23] Temperature fields in the APT symmetric diffusive system (convection velocity $v \leq v_{\mathrm{EP}}$) reach a dynamically localized state, where the phase (position of maximum temperature) difference is fixed and the amplitude (temperature gradient) distribution is balanced between the two channels. Due to the fact that the heat and temperature are actually not equivalent, one can acquire asymmetric couplings of temperature fields by directly contacting the channels of different materials without breaking the reciprocal law of heat conduction.[27] In this way, the amplitude distribution can be easily modulated by adjusting the mass densities of channels. On this basis, the tight-binding non-Hermitian Su–Schrieffer–Heeger model with the asymmetric coupling was proposed and the diffusive skin effect was proved.[31−34] Different from the symmetrically coupled system,[29,30] where bulk modes and edge modes can be clearly distinguished, all the modes in asymmetrically coupled systems will localize at the edges under the open boundary condition, which is termed diffusive skin effect.

In this Letter, we focus on coupled-ring systems which involve both thermal convection and asymmet-

*Corresponding authors. Email: eleying@zju.edu.cn; xfzhu@hust.edu.cn
© 2022 Chinese Physical Society and IOP Publishing Ltd

ric couplings. In the asymmetrically coupling double-channel model, we find that the temperature field is also asymmetrically distributed and phase locked at the convection velocity $v \leq v_{\rm EP}$. In the multiple-channel tight-binding chains, the phase-locking effect in the convection-driven particle-hole symmetric diffusive system and the skin effect in the asymmetric-coupling-based sublattice symmetric diffusive system are discussed. Here, the diffusive skin effect can be regarded as a result of the asymmetric temperature field distributions in the symmetry broken phase at the convection velocity $v > v_{\rm EP}$. It should be noted that the diffusive skin effect is generated in the passive thermal system at the steady state, which is different from the geometric heat pump effect in the periodic time-driven active system at the transient state.[35–37] In the end, we prove the phase-locking diffusive skin effect by combining the complex thermal convection and the asymmetric coupling. Our work shows a unique temperature field modulation mechanism in coupling diffusive systems, which shows the prospective potentials in thermal topology. The existence of high-order EPs may also be important in the precise thermal sensing.[21,38]

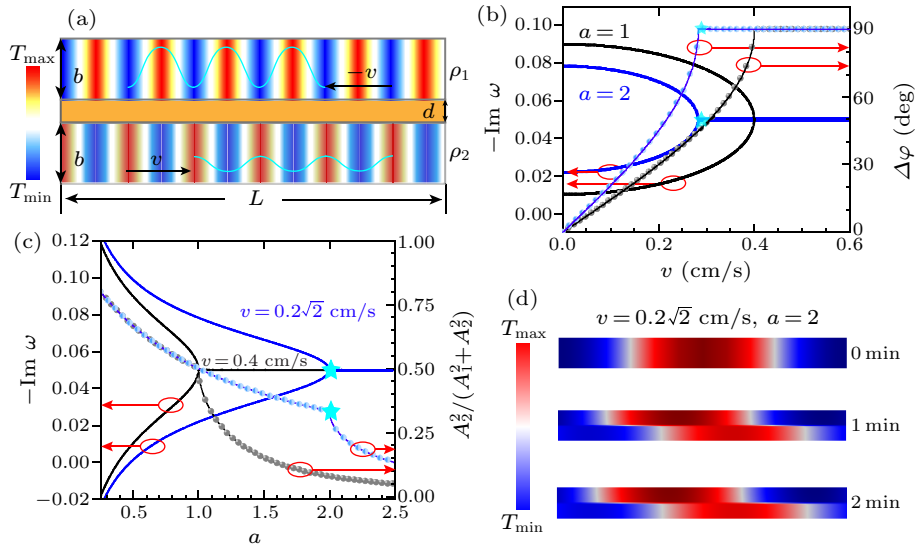

Fig. 1. (a) A schematic of the double-channel system with opposite convection and asymmetric coupling. In (a), the convection velocity is v $(-v)$ and the asymmetric coupling is determined by the mass density ratio $a=\rho_2/\rho_1$. The temperature field is asymmetrically distributed and phase locked in channels. (b) Decay rate $(-\mathrm{Im}\omega)$ and the phase difference $(\Delta\phi)$ vs the convection velocity. Here, $\Delta\phi$ can be engineered from 0 to $\pi/2$ continuously. (c) Decay rate and intensity distribution vs the asymmetric coupling. The temperature field tends to localize in the channel with a smaller density. (d) Temperature field evolution at $v=v_{\rm EP}$ in the coupled channels, where the phase difference is $\pi/2$ [the star marks in (b)] and the intensity ratio between upper and lower channels is $A_1^2/A_2^2=2/1$ [the star marks in (c)] for the steady state.

As schematically shown in Fig. 1(a), two channels with different mass densities $(\rho_{1,2})$ are moving oppositely in the velocities of $\mp v$. The length and width of channels are denoted by L and b. The temperature fields $T_{1,2}$ in the upper and lower channels are dynamically localized with a fixed phase difference and unbalanced amplitudes. The process of temperature field coupling can be described by the diffusive coupled mode theory. The temperature field can be regarded as being periodically distributed in the ring structure, which can be given in a wave-like form solution as $T=Ae^{i(\beta x-\omega t)}+T_0$.[23] Here, A is the amplitude of temperature field, which represents the temperature gradient in the channel. Here, $\beta=\frac{2m\pi}{L}$ is the propagating constant, ω is the decay rate, and T_0 is the reference temperature. In this study, we take the first-order mode $m=1$ and set $T_0=0$ for convenience. Deducing from Fourier's law in heat conduction, we can obtain the coupled mode equation[23]

$$\rho_{1,2}C_{1,2}\frac{\partial T_{1,2}}{\partial t}=\kappa_{1,2}\frac{\partial^2 T_{1,2}}{\partial x^2}\pm\rho_{1,2}C_{1,2}v\frac{\partial T_{1,2}}{\partial x}+h_{\rm s1,s2}, \tag{1}$$

where $C_{1,2}$, $T_{1,2}(x,t)$ and $\kappa_{1,2}$ are the heat capacities, temperature fields and thermal conductivities in the upper and lower channels. In Eq. (1), t represents the time and x is the convection axis. $T_{1,2}(x,t)$ can be regarded to be uniform along the coupling axis, since the thermal channel is narrow. According to the continuity conditions of temperature field (T) and heat flux (q) at the upper and lower boundaries of the coupling interlayer, one can obtain $T_{iu}=T_1$, $T_{id}=T_2$, $q_{iu}=q_1$, and $q_{id}=q_2$. Heat exchange in the coupled channels can thus be deduced as $h_{\rm s1,s2}=\frac{q_{1,2}}{b}=\frac{\kappa_i\Delta T_{1,2}}{bd}$ with the exchange rates $h_{1,2}=\frac{\kappa_i}{\rho_{1,2}C_{1,2}bd}$. Here, κ_i and d represent the thermal conductivity and the thick-

ness of the interlayer. Equation (1) can thus be transformed into an eigen-problem of $H|\Psi\rangle = \omega|\Psi\rangle$, with H and $|\Psi\rangle$ being the effective Hamiltonian and the eigenstates of $(A_1, A_2)^{\mathrm{T}}$,[23]

$$H = \begin{pmatrix} -i(\beta^2 D_1 + h_1) + \beta v & ih_1 \\ ih_2 & -i(\beta^2 D_2 + h_2) - \beta v \end{pmatrix}, \tag{2}$$

where $D_{1,2} = \frac{\kappa_{1,2}}{\rho_{1,2} C_{1,2}}$ are the diffusivities. Note that $PTH = -HPT$ is satisfied only at $h_1 = h_2$, indicating that the Hamiltonian is not APT symmetric in a general case. From Eq. (2), eigenvalues can be calculated by

$$\omega_{\pm} = -i(S_0 \pm \sqrt{h_1 h_2 - \beta^2 v^2}\,), \tag{3}$$

where S_0 is the unified decay rate of each channel by adjusting $\kappa_{1,2}$ to get the sum of $\beta^2 D_{1,2} + h_{1,2} = S_0$. Eigenvectors are

$$u_{\pm} = \left(\pm\sqrt{h_1/h_2}\, e^{\pm i\phi}, 1\right)^{\mathrm{T}}, \ (v = v_{\mathrm{EP}} \sin\phi \leqslant v_{\mathrm{EP}}),$$
$$u_{\pm} = \left(\pm\sqrt{h_1/h_2}\, e^{\pm\varphi}, i\right)^{\mathrm{T}}, \ (v = v_{\mathrm{EP}} \cosh\varphi \geqslant v_{\mathrm{EP}}). \tag{4}$$

From Eqs. (3) and (4), the EP locates at $v_{\mathrm{EP}} = \frac{\sqrt{h_1 h_2}}{\beta}$, where eigenvalues and eigenvectors are both degenerated. In the state before the EP ($v \leqslant v_{\mathrm{EP}}$), the eigenvalues are imaginary and the coupling dominates the process of diffusion. In this case, phase difference $\Delta\phi$ is only related to the convection velocity v, and the amplitude keeps at $\sqrt{h_1/h_2} = \sqrt{\rho_2/\rho_1} = \sqrt{a}$. In the state after the EP ($v \geqslant v_{\mathrm{EP}}$), eigenvalues begin to have real parts. $\Delta\phi$ holds at $\pi/2$ and $\sqrt{h_1/h_2}$ varies with the convection.

In Figs. 1(b)–1(d), we give a numerical simulation example, where the structural parameters are set to be $b = 12.5\,\mathrm{mm}$, $d = 2\,\mathrm{mm}$, $L = 0.2\pi\,\mathrm{m}$, ($R \approx 0.1\,\mathrm{m}$ for 3D ring cases). The thermal conductivities, mass densities, and heat capacities of channels are $\kappa_{1,2} = 100\,\mathrm{W/(m{\cdot}K)}$, $\rho_{1,2} = 1000\,\mathrm{kg/m^3}$, $C_{1,2} = 1000\,\mathrm{J/(kg{\cdot}K)}$, while the ones of the coupling layers are $\kappa_i = 1\,\mathrm{W/(m{\cdot}K)}$, $\rho_i = 1000\,\mathrm{kg/m^3}$, $C_i = 1000\,\mathrm{J/(kg{\cdot}K)}$. In Fig. 1(b), we find that there exist EPs for both symmetric coupling and asymmetric coupling cases. Under the condition of eigenstate excitation, the phase difference between the two coupled ring channels changes from 0 to $\pi/2$ at $v = 0 \to v_{\mathrm{EP}}$ and keeps $\pi/2$ at $v > v_{\mathrm{EP}}$. Here, the EPs locate at $v_{\mathrm{EP}} = 0.4\,\mathrm{cm/s}$, $0.2\sqrt{2}\,\mathrm{cm/s}$, when $a = 1, 2$, respectively. In Fig. 1(c), the intensity distributions of temperature fields (A_1^2 and A_2^2) in channels 1 and 2 are presented. Interestingly, the intensity distributions of temperature fields in the upper and lower channels can be modulated from near 0/1 to almost 1/0 in succession, which is balanced at 0.5/0.5 with the symmetric couplings of $a = 1$. For each case, the EP connects the regions of different intensity change rates with respect to the variation of mass density ratio. In Fig. 1(d), we present the transient temperature field evolution in the channels, when $v = v_{\mathrm{EP}} = 0.2\sqrt{2}\,\mathrm{cm/s}$ and $a = 2$. The result shows that the temperature field reaches a steady state finally, with the phase lag fixed at $\pi/2$ and the field amplitude clearly asymmetric.

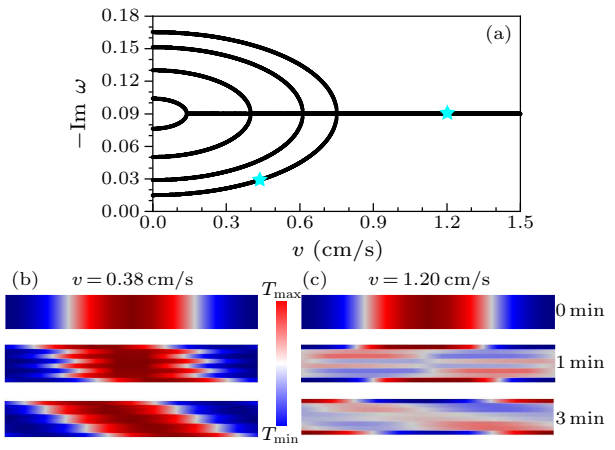

Fig. 2. Convection-induced phase-locking effect in one-dimensional (1D) coupled thermal channels of the particle-hole symmetry. (a) Decay rate vs the convection velocity. (b) Phase locking effect for the uniform excitation before the EP at $v = 0.38\,\mathrm{cm/s}$, as marked by the star in (a). (c) Boundary localization of temperature fields, for the uniform excitation after the EP at $v = 1.20\,\mathrm{cm/s}$, as marked by the star in (a). Note that the excited branch of the eigenstate is in the lowest decay rate, and the phases are unlocked in the case after the EP. In simulations, the number of channels is $N = 8$.

Here, we extend the double-channel model into the 1D non-Hermitian tight-binding lattice for the investigation of complex dynamics of heat conduction. We firstly focus on the phase and amplitude evolution in the convection-modulated multiple-channel model. The Hamiltonian takes the form[39]

$$H_1 = [-iS_0 + (-1)^n \beta v] \sum_{n=1}^{N} |n\rangle\langle n| + ih_0 \sum_{n=1}^{N-1} (|n\rangle\langle n+1| + |n+1\rangle\langle n|), \tag{5}$$

where n is the site number. As the extension of the double-channel model, the adjacent channels in this multiple-channel system have the opposite convection velocities of $\pm v$ and symmetric couplings of ih_0 ($a = 1$). The onsite diffusivities of all channels can be unified as $-iS_0$, so that the diffusive system satisfies the particle-hole symmetry.[39] As we know, the excited state in practice is always the eigenstate with the lowest decay rate. In Fig. 2(a), we choose to excite the eigenstates on the branch of the lowest decay rate as marked by the stars at different phases. Our results clearly show that for the uniform excitation, the system is phase locked and the amplitude distribution is very stable in the steady state at the phase

before the EP of $v = 0.38\,\mathrm{cm/s}$. As shown in Fig. 2(b), the lag phase is $\Delta\phi = \pi/6$. In the phase after the EP of $v = 1.20\,\mathrm{cm/s}$, the system under the uniform excitation renders an edge field localization without a stable phase difference between the coupling channels, as shown in Fig. 2(c). It should be emphasized that the convection-induced edge localization of temperature fields in this case is not topologically protected, which can be disturbed by convection disorders.

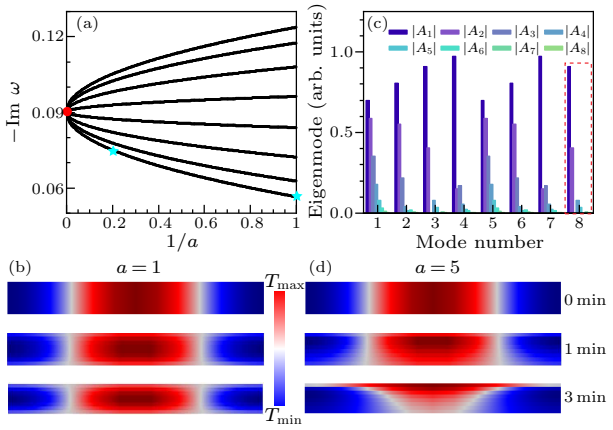

Fig. 3. Asymmetric-coupling-induced diffusive skin effect in the sublattice symmetric system, which can be regarded as a result of unbalanced temperature field distributions in the broken phase after the high-order EP. (a) Decay rate vs the mass density ratio of $1/a$. The red dot denotes the existence of a high-order EP, when the asymmetric coupling between adjacent channels is unidirectional. (b) Temperature field evolution for the uniform excitation of eigenstates with the lowest decay rate in the symmetric coupling case ($1/a = 1$), as marked by the star in (a). (c) Eigenfield distributions of all the eight eigenstates at the asymmetric coupling of $1/a = 0.2$. (d) Temperature field evolution for uniform excitation in the asymmetric coupling case ($1/a = 0.2$), as marked by the star in (a).

In the next part, we choose the Hatano–Nelson model[40] with only asymmetric couplings between adjacent channels to investigate the asymmetric-coupling-induced amplitude modulation as well as high-order EPs. For the case in Fig. 3, the Hamiltonian of N asymmetrically coupled channels can be expressed as

$$H_2 = -iS_0\sum_{n=1}^{N}|n\rangle\langle n| + \sum_{n=1}^{N-1}(ih_1|n\rangle\langle n+1| + ih_2|n+1\rangle\langle n|). \quad (6)$$

From the Hamiltonian, the system respects the sublattice symmetry with $\hat{\sigma}_z^{-1}(H_2+iS_0\hat{I})\hat{\sigma}_z = -(H_2+iS_0\hat{I})$, which ensures that the eigenvalues are obtained in pairs as $iS_0 \pm \omega$. Here, $\hat{\sigma}_z$ is the Pauli matrix and $\hat{I}$ is the identity matrix. From Eq. (6), we find that an Nth order EP can be generated when the coupling is completely asymmetric or unidirectional, for example, with $h_1 \neq 0$ and $h_2 = 0$, as marked by the red sphere in Fig. 3(a). In Fig. 3(b), we show the temperature field evolution for uniform excitation of the eigenstate in the symmetric coupling case of $a = 1$ for comparison. The steady state at $t = 5\,\mathrm{min}$ is featured with the temperature field concentration in the central region. When $a = 5$, by analyzing the eigenmodes from Eq. (6), we can find that the temperature fields of all eigenmodes tend to gather in the first channel. As shown in Fig. 3(c), in similarity to the well-known non-Hermitian skin effect in wave systems.[31–34] The absolute of eigenmode $|\Psi\rangle = [1, a^{-\frac{1}{2}}, 0, a^{-\frac{3}{2}}, a^{-\frac{4}{2}}, 0, a^{-\frac{6}{2}}, a^{-\frac{7}{2}}]^{\mathrm{T}}$ is at the lowest decay rate, with an amplitude gradient of $a^{-\frac{1}{2}}$ in adjacent channels. Figure 3(d) shows the transient temperature field evolution for uniform excitations in the asymmetric coupling case of $a = 5$. Our results show that at the steady state ($t = 5\,\mathrm{min}$), the temperature field becomes localized at the boundary. According to the non-Bloch mode theory, Eq. (6) can be equivalently transformed into a Hermitian form in the momentum space. By translating the Bloch vector with an imaginary component of $K \to K + i\ln a$,[31] the asymmetric coupling induced complex potential can be eliminated.

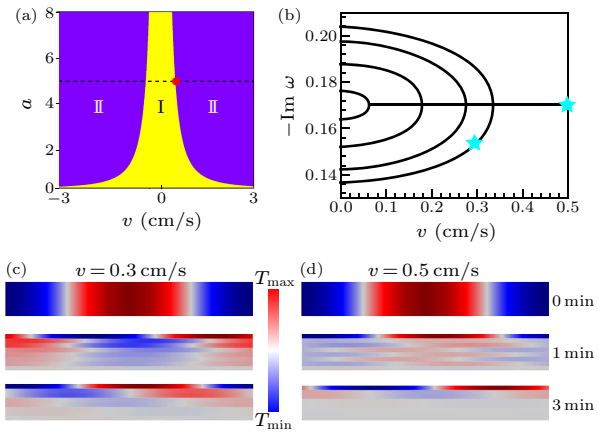

Fig. 4. The phase-locking diffusive skin effect. (a) Phase diagram vs the convection velocity and asymmetric coupling. Phase I before the EP [at the branch with the lowest decay rate in (b)] is distinguished from the phase Ⅱ after the EP by different colors. (b) Decay rate at the asymmetric coupling $a = 5$ vs the convection velocity. (c) Phase-locking diffusive skin effect at phase I. (d) Diffusive skin effect at the phase Ⅱ, where phase difference between the adjacent channels is no longer locked. The cases in (b)–(d) locate on the dashed line in (a), where the red dot in (a) denotes an EP.

Here, we present the diffusive skin effect in a tight-binding ring structure. The mass densities of on-site rings need to be adjusted by using different metamaterials in direct contact to achieve the asymmetric coupling. The thermal conductivities of coupling layers also need to be modulated to normalize the decay rates. For the experimental implementation, we

can use the ball-stick model with only the coupling strength concerned. The changing on-site mass densities and off-site thermal conductivities can be realized through the equivalent medium filling. We can further investigate the high-order diffusive skin effect by extending the model into higher dimensions. Different from the diffusive skin effect in 1D ring structures, where the temperature field tends to be localized at the boundary with the maximum gradient, the diffusive skin effect in 2D lattice structures is predicted to render as the corner states with the corner site having the maximum temperature.

It is intuitive to obtain that both phase and amplitude modulations of temperature field can be realized by tailoring the convection velocity and asymmetric coupling. In the last part, we study the non-Hermitian lattice with Hamiltonian

$$H_3 = [-iS_0 + (-1)^n \beta v] \sum_{n=1}^{N} |n\rangle\langle n| + \sum_{n=1}^{N-1} (ih_1 |n\rangle\langle n+1| + ih_2 |n+1\rangle\langle n|), \quad (7)$$

where both the onsite convection in each channel and the asymmetric coupling between adjacent channels are considered. Figure 4(a) shows the phase diagram in relation to the convection velocity and asymmetric coupling, where the different phases are clearly presented. Here we focus on the asymmetric coupling case of $a = 5$, as marked by the dashed line in Fig. 4(a). The decay rate of the whole system at $a = 5$ is shown in Fig. 4(b). The results show that due to the existence of thermal convection, the original Nth order EP in the static system of the sublattice symmetry will split into four second-order EPs. Here we excite the eigenmodes on the branch of the lowest decay rate as marked by the stars in Fig. 4(b). In phase I before the EP at $v = 0.3\,\mathrm{cm/s}$ [Fig. 4(c)], we find that the phase-locking diffusive skin effect is emerged, for which the temperature fields in adjacent channels have a fixed phase lag and an edge localization of the amplitude distribution. However, in phase II after the EP at $v = 0.5\,\mathrm{cm/s}$ [Fig. 4(d)], the phases of temperature fields in each channel become disorder without an apparent locking due to the large thermal convection. It needs to be mentioned that the diffusive skin effect is robust and still holds.

In conclusion, we show the important role of convection and asymmetric couplings for the phase and amplitude modulation of temperature fields in the coupled thermal systems. From the non-Hermitian Hamiltonians by extending the double-channel model into the 1D tight-binding multiple-channel model, we reveal the phase-locking effect in the particle-hole symmetric diffusive systems with convection modulation. We also prove the existence of high-order EPs and diffusive skin effect in the sublattice symmetric diffusive systems with asymmetric coupling modulation. By combining the convection and asymmetric couplings, our results show that there exists the phase-locking diffusive skin effect, for which the phase differences between adjacent channels are locked and the temperature field amplitude becomes localized on the edge of the non-Hermitian lattice.

For the diffusive skin effect with large temperature gradients localized at the boundary, our proposed system may produce a strong thermoelectric effect for the thermoelectric power generation and heat harvesting. Since the EP is a point where both eigenvalues and eigenvectors degenerated, any perturbation will lead to spectrum splitting at this singularity point. One can theoretically prove that the spectrum splitting obeys the rule of $\Delta(\mathrm{Re}\omega_{\pm}) \propto \epsilon^{1/n}$, where $\omega_{\pm}$ are the eigenvalues at the two splitting branches, ϵ is the perturbation strength of defects, and n is the degeneracy order of EP. Therefore, one can detect the perturbation by measuring the phase changes with or without the spectrum splitting. The proposed phase-locking diffusive skin effect provides a unique approach in manipulating the heat conduction in coupled diffusive systems and have the potential applications in the thermal sensing, heat harvesting, and thermal functional devices with topological protection.

Acknowledgments. This work was supported by the National Natural Science Foundation of China (Grant Nos. 92163123, 11690030, and 11690032).

References

[1] Schittny R, Kadic M, Guenneau S and Wegener M 2013 *Phys. Rev. Lett.* **110** 195901
[2] Li Y *et al.* 2021 *Nat. Rev. Mater.* **6** 488
[3] Yang S, Wang J, Dai G, Yang F and Huang J P 2021 *Phys. Rep.* **908** 1
[4] Yu X *et al.* 2021 *Chin. Phys. Lett.* **38** 014401
[5] Song Q *et al.* 2016 *Nanoscale* **8** 14943
[6] Feng H *et al.* 2019 *J. Phys. Chem. C* **123** 31003
[7] Fan C, Gao Y and Huang J P 2008 *Appl. Phys. Lett.* **92** 251907
[8] Han T, Bai X, Thong J, Li B and Qiu C W 2014 *Adv. Mater.* **26** 1731
[9] Peng Y G, Li Y, Cao P C, Zhu X F and Qiu C W 2020 *Adv. Funct. Mater.* **30** 2002061
[10] Li Y *et al.* 2015 *Phys. Rev. Lett.* **115** 195503
[11] Li Y *et al.* 2019 *Nat. Mater.* **18** 48
[12] Torrent D, Poncelet O and Batsale J 2018 *Phys. Rev. Lett.* **120** 125501
[13] Li J *et al.* 2022 *Nat. Commun.* **13** 167
[14] Li Y, Li J, Qi M, Qiu C W and Chen H 2021 *Phys. Rev. B* **103** 014307
[15] Xu L, Huang J P and Ouyang X 2021 *Appl. Phys. Lett.* **118** 221902
[16] Bender C M 2007 *Rep. Prog. Phys.* **70** 947
[17] Zhu X F, Ramezani H, Shi C, Zhu J and Zhang X 2014 *Phys. Rev. X* **4** 031042
[18] Gu Z *et al.* 2021 *Phys. Rev. Appl.* **16** 057001
[19] Li Z *et al.* 2021 *Prog. Electromagn. Res.* **171** 1

[20] Shi C *et al.* 2016 *Nat. Commun.* **7** 11110
[21] Wang S *et al.* 2019 *Nat. Commun.* **10** 832
[22] Longhi S, Gatti D and Valle G D 2015 *Phys. Rev. B* **92** 094204
[23] Li Y *et al.* 2019 *Science* **364** 170
[24] Cao P C, Li Y, Peng Y G, Qiu C W and Zhu X F 2020 *ES Energy Environ.* **7** 48
[25] Xu L, Dai G, Wang G and Huang J P 2020 *Phys. Rev. E* **102** 032140
[26] Cao P C *et al.* 2021 *Chin. Phys. B.* **30** 030505
[27] Cao P C *et al.* 2021 *Commun. Phys.* **4** 230
[28] Xu G, Li Y, Li W, Fan S and Qiu C W 2021 *Phys. Rev. Lett.* **127** 105901
[29] Qi M *et al.* 2021 arXiv:2107.05231
[30] Xu G, Yang Y, Zhou X *et al.* 2022 *Nat. Phys.* (accepted)
[31] Yao S and Wang Z 2018 *Phys. Rev. Lett.* **121** 86803
[32] Okuma N, Kawabata K, Shiozaki K and Sato M 2020 *Phys. Rev. Lett.* **124** 86801
[33] Weidemann S *et al.* 2020 *Science* **368** 311
[34] Yan Q, Chen H and Yang Y 2021 *Prog. Electromagn. Res.* **172** 33
[35] Ren J, Hänggi P and Li B 2010 *Phys. Rev. Lett.* **104** 170601
[36] Ren J, Liu S and Li B 2012 *Phys. Rev. Lett.* **108** 210603
[37] Wang Z *et al.* 2022 *Front. Phys.* **17** 13201
[38] Wiersig J 2014 *Phys. Rev. Lett.* **112** 203901
[39] Mostafavi F *et al.* 2020 *Phys. Rev. Res.* **2** 0320570
[40] Hatano N and Nelson D R 1996 *Phys. Rev. Lett.* **77** 570